MECH0064 MSc Group Design Project

Compact Continuum Robotic Manipulator Platform

Group members:

Zehao Ye (23119333) Yuhao Zhu (23041703)

Zehao Ye (23119333) Zehao Ye (23119333)

Zehao Ye (23119333) Zehao Ye (23119333)

Supervised by **Dr Reza Haqshenas**

Abstract

This is the Abstract of the final report.

AAAAA bbb

test for github

Key Words: Continuum Robotic e.g.

Contents

List of Figures

List of Tables

1 Introduction

Introduction including market survey.

Introduction including market survey.

1.1 Background

This is the background part.

1.2 Motivation

This is the motivation part.

2 Literature Review

This is the Literature Review of the final report.

2.1 Introduction

Continuum robots has emerged and attracted a lot of attention since 2008 [6]. Compared with traditional rigid joint manipulator, continuum robots stand out for their flexible, highly bendable structure and extremely flexible motion performance. This new kind of robot not only changes the code of traditional robot design but also demonstrates unprecedented application potential in fields such as medical science [4]. Meanwhile, rigid-flexible- soft coupled continuum robots combine the multiple advantages of the stability of rigid structures, the flexibility of flexible structures, and the compliance of soft structures, and are one of the most promising robots for increasingly complex tasks [9].

During the development process of robotic science, the limitations of rigid joint robots have gradually shown up, especially in applications requiring highly detailed operation and in complex or space-limited environments. With unique bionic structure and motion characteristics, continuum robots provide new possibilities to solve these challenges.

This paper will discuss different types of existing continuum robots and their working principles, advantages, and disadvantages, then propose a proper continuum robot design that can be mainly applied to medical FUS applications.

2.2 Working Principles

Continuum robot can be broadly divided into two parts: a continuous bending structure and a fixed base containing actuating and controlling devices. In continuum robots, the key element is their backbone which runs through the whole structure and defines the basic shape of, making bending and rotating movement possible [8].

The user manipulates the robot by controlling the actuator in the base part. Flexible elements such as tendons and springs distributed around the backbone are connected to the actuator and can transmit bending and rotation movements

along the robot body, even expansion.

Figure 1: ***An example of continuum robot*** [7].

Different types of continuum robots have different backbones, actuating and flexible components, but they are generally all work under the same working principle stated above.

2.3 Types of Continuum Robots

Nowadays, a variety of continuum robots exist, each exhibiting unique structures and functions. They serve in different fields such as medicine, construction, and exploration. In this section, some of the most popular continuum robots will be introduced, providing basic insights into their structures as well as discussing their merits and drawbacks.

2.3.1 Tendon-Driven Robots

The arm of the Tendon-Driven robot consists of a backbone, several tendons and disks. The backbone defines the structure and posture of the entire robot arm, while disks define the diameter and divide the robot arm into segments, and tendons are stretched to create deformation and movements of different directions for the robot arm.

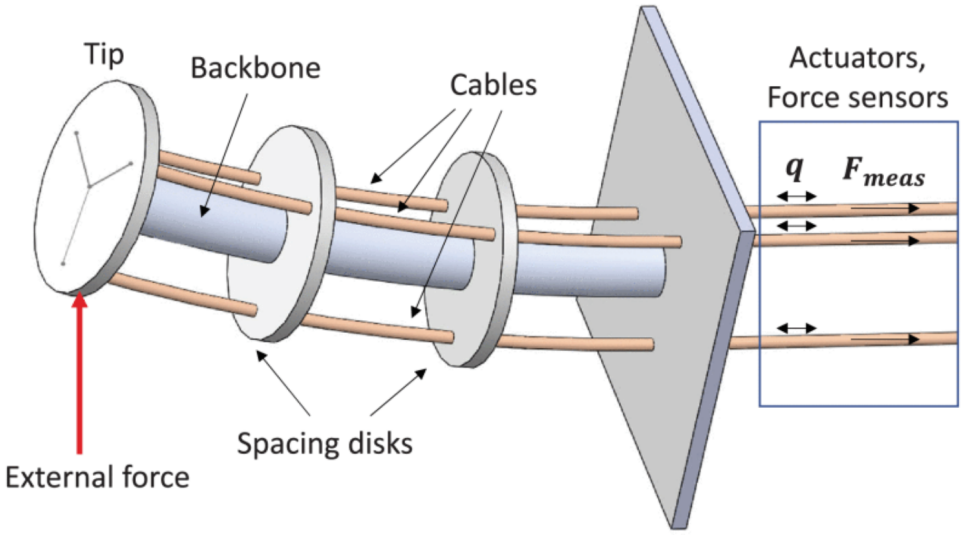

Figure 2: ***The three tendons continuum robot with one segment*** [5].

Figure 2 shows only the simplest tenon-driven robots. In practical applications, there may be more than one backbone, and the disks are not necessarily parallel. Compared with other continuum robots, one of the most significant advantages of tendon-driven robots is their flexibility. This advantage makes it more effective in performing tasks in complex and restrictive Spaces. In addition, due to the simple components needed to construct the robot, it is easier to meet lightweight design specifications. Moreover, like the concentric-tube continuum robots, tendon-driven continuum robots can be built designed on a small scale with diameters of below 10mm [1].

However, due to its simple actuating principle, more complex algorithms are needed to control it more accurately. Also, the tendon-driven robots actuate by pulling the tendon, which makes the friction between the tendon and other components inevitable, which will accelerate the wearing speed of the

tendon-driven robots.

2.3.2 Fishbone Robots

The fishbone robots are inspired by fishbones. It is comprised of multiple "fishbone units" which consist of rigid cross-shaped plates and soft rubber sleeves, with a layer of manganese alloy steel elastic plate embedded in the middle to form a rigid-soft coupled structure[9]. In contract to the existing single-backbone continuum robots, the middle backbone of the continuum robot is serially formed by multiple cross- arranged bioinspired fishbone units. The fishbone units stack layer by layer, forming a spine-like shaper. Like tendon-driven robots, it utilizes cables to simulate muscle movement, causing layers of fishbones to bend in corresponding directions through cable stretching at different positions.

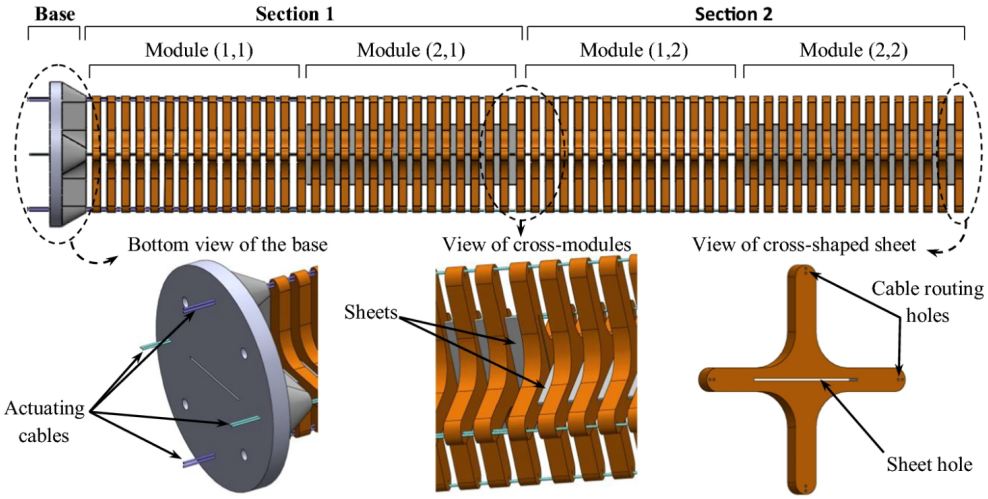

Figure 3: ***The cable-driven fish bone continuum robot with cable arrangement*** [2].

Because many fishbone units are stacked together as the backbone of the fishbone continuum robots, the structural stability of this kind of robot is very strong. The disadvantage, however, is that it is difficult to make lightweight designs since the density of the components is high.

2.3.3 Concentric Tube Continuum Robots

concentric tube robots, shaped like retractable walking sticks, consist of many tubes with decreasing diameters. Each tube is nested on top of the previous wider

tube.

The concentric robots are made of two parts: tubes and coaxial actuation units. The tubes are the main structural element of this robot and act as the backbone. The coaxial actuation unit consists of two motors which are responsible for rotation and translation movement respectively. Each tube is actuated by an independent coaxial actuation unit.

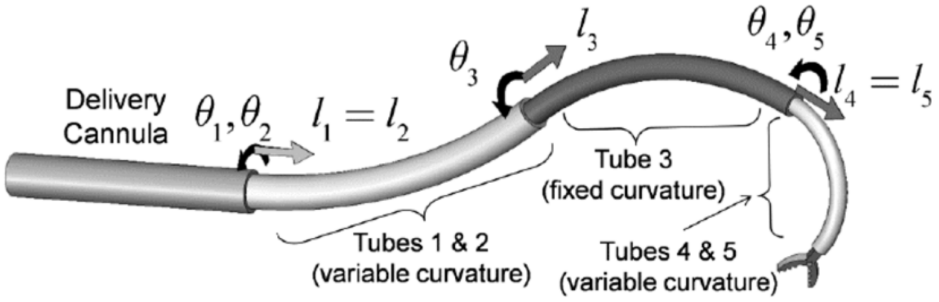

Figure 4: ***An example concentric tube continuum robot*** [3].

The most significant advantage of this kind of robots is that of all the continuum robots, concentric tube robots have the smallest possible outer diameter and are best suited to work in confined and narrow Spaces. Therefore, it is the ideal choice for surgical operations.

Their disadvantages, on the other hand, are also very evident. Since each tube requires an independent actuation unit, the overall length of the robot cannot be very long, because longer lengths will lead to more tubes, and will lead to more tip position errors.

3 Design

This is the Design of the final report.

3.1 Methodology

3.1.1 Forward Kinematics

The manipulator consists of four units, and the backbones of each section are perpendicular to each other. To derive the workspace of the manipulator for further analysis, the forward kinematics formula need to be conducted. According to the fishbone continuum robot[9], the forward kinematics formula of two perpendicular units are shown in Equations 1, 2, and 3.

$$\begin{aligned} x = &- \frac{S_r r}{\Delta S_1} + \frac{S_r r}{\Delta S_1} \cos\left(\frac{\Delta S_l}{r}\right) - d_1 \sin\left(\frac{\Delta S_l}{r}\right) \\ &- \frac{S_r r}{\Delta S_3} \sin\left(\frac{\Delta S_1}{r}\right) \sin\left(\frac{\Delta S_3}{r}\right) \\ &- d_2 \sin\left(\frac{\Delta S_1}{r}\right) \cos\left(\frac{\Delta S_3}{r}\right) \end{aligned} \tag{1}$$

$$y = -\frac{S_r r}{\Delta S_3} + \frac{S_r r}{\Delta S_3} \cos\left(\frac{\Delta S_3}{r}\right) - d_2 \sin\left(\frac{\Delta S_3}{r}\right) \tag{2}$$

$$\begin{aligned} \mathrm{Z} = &\frac{S_r r}{\Delta S_1} \sin\left(\frac{\Delta S_\mathrm{l}}{r}\right) + d_1 \cos\left(\frac{\Delta S_\mathrm{l}}{r}\right) \\ &+ \frac{S_r r}{\Delta S_3} \sin\left(\frac{\Delta S_3}{r}\right) \cos\left(\frac{\Delta S_1}{r}\right) \\ &+ d_2 \cos\left(\frac{\Delta S_1}{r}\right) \cos\left(\frac{\Delta S_3}{r}\right). \end{aligned} \tag{3}$$

However, calculating the centroid directly using the above formula becomes complex while there are four units in the manipulator. Additionally, the inverse kinematics part also requires the derivation of corresponding matrices for subsequent calculations using the composite coordinate transformation formula. Therefore, The relevant matrices for subsequent calculations need to be derived. According to the design specifications, the manipulator comprises four units.

The backbones of the units are vertically aligned. The base coordinate system can be established with the centroid of base disk upper surface serving as the origin. The x-axis of the coordinate system is aligned with the backbone of the unit nearest to the base disk. Consequently, the backbones of units 1 and 3 are parallel to the x-axis, while those of units 2 and 4 are parallel to the y-axis. The positions of the five centroids in the base coordinate system when the manipulator is in the initial position are shown in Figure 5. The centroids of the five disc upper surfaces are designated as $node_1$, $node_2$, $node_3$, $node_4$, and $node_5$.

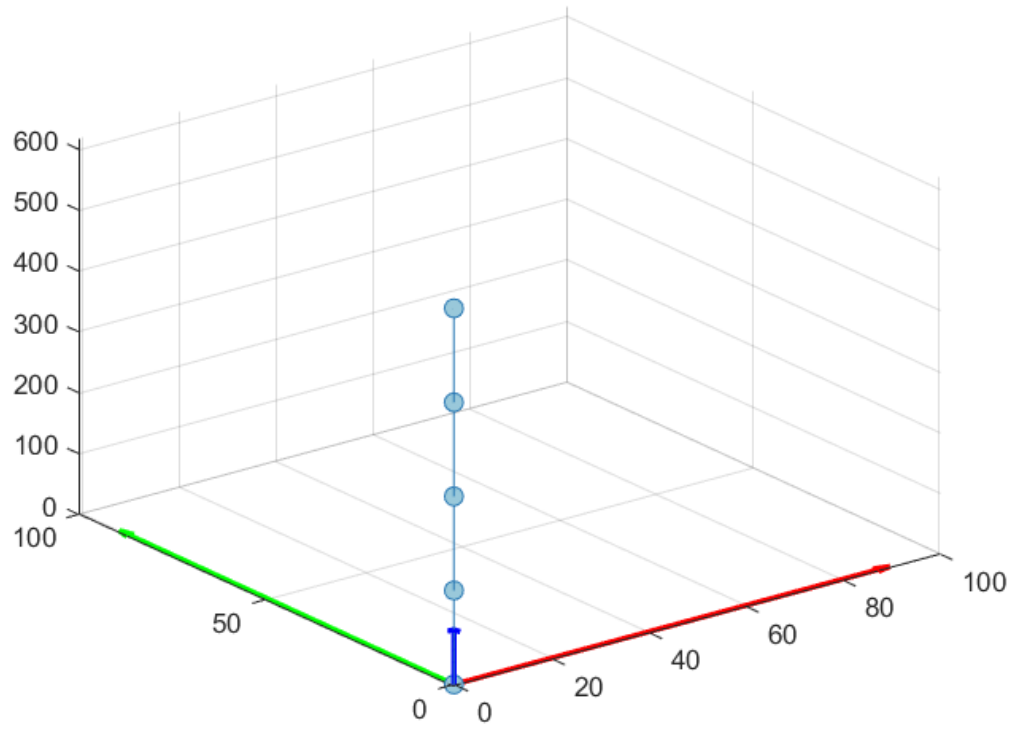

Figure 5: ***The kinematics model of manipulator in initial position.***

The unit 1 is restricted to bending in the y-z plane of the coordinate system where $node_1$ serves as the origin, while the unit 2 is restricted to bending in the x-z plane of the coordinate system where $node_2$ serves as the origin. Similarly, the unit 3 and unit 4 are subject to the same constraints. The bending angles for these units are defined as α_1, α_2, α_3, and α_4, respectively. The positions of the manipulator model in the base coordinate system after bending each unit by 90° are illustrated in Figure 6.

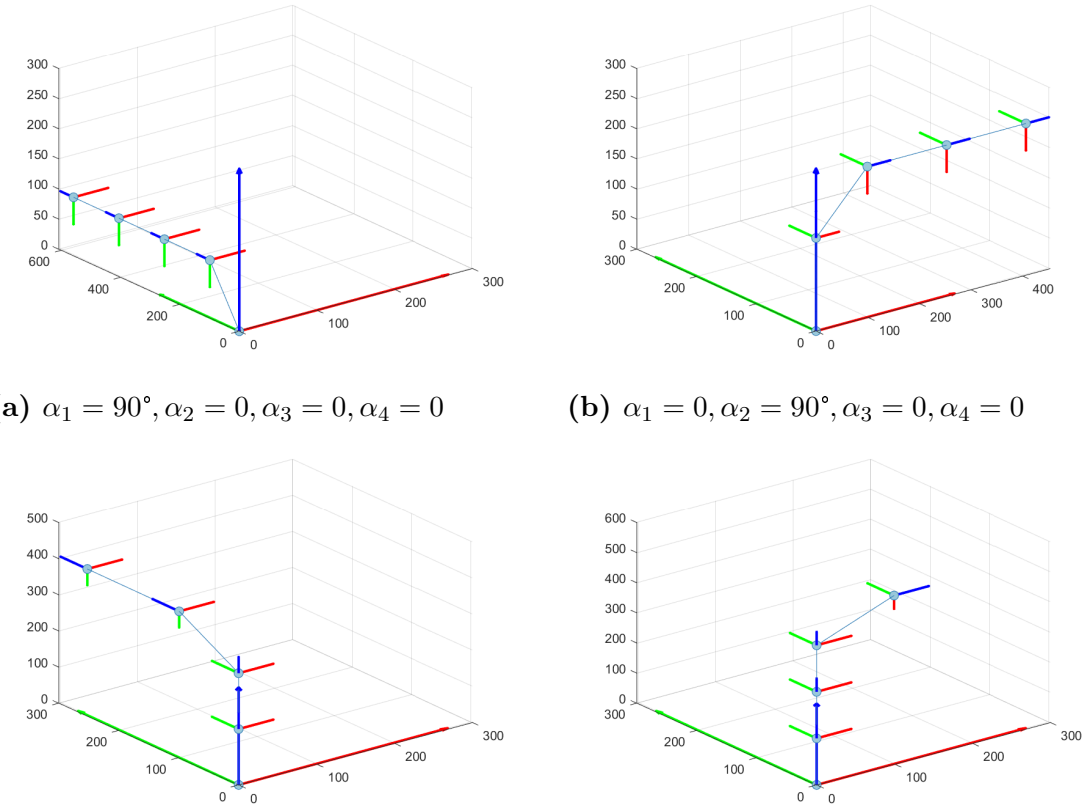

(a) $\alpha_1 = 90°, \alpha_2 = 0, \alpha_3 = 0, \alpha_4 = 0$

(b) $\alpha_1 = 0, \alpha_2 = 90°, \alpha_3 = 0, \alpha_4 = 0$

(c) $\alpha_1 = 0, \alpha_2 = 0, \alpha_3 = 90°, \alpha_4 = 0$

(d) $\alpha_1 = 0, \alpha_2 = 0, \alpha_3 = 0, \alpha_4 = 90°$

Figure 6: ***The kinematics model of manipulator with respective bending units.***

While the units bend to the positive direction of x-axis or y-axis, the bending angles α are positive. Owing to the distinct properties of the four units, different calculation methods are required for analysis. The unit i have a base node $node_i$ and an end effector node $node_{i+1}$. To further calculate the position of $node_{i+1}$ in the base coordinate system, these matrices can be employed in the Equation 4.

$$\mathbf{P}_{i+1}^{base} = \mathbf{B}_i \times \mathbf{P}_{i+1}^{i} + \mathbf{P}_{i}^{base} \tag{4}$$

$\mathbf{P}_{i+1}^{base}$: The position of $node_{i+1}$ in the base coordinate system.

$\mathbf{B}_i$: The rotational matrix tranforms the base coordinate system into coordinate system i, which is the coordinate system with origin $node_i$.

$\mathbf{P}_{i+1}^{i}$: The position of $node_{i+1}$ in coordinate system i.

$\mathbf{P}_{i}^{base}$: The position of $node_i$ in the base coordinate system.

- Unit 1

  For Unit 1, the relationship between the relative position matrix of $node_1$ and $node_2$ $\mathbf{P}_2^1$ and α_1 is shown in Equation 5.

$$\mathbf{P}_2^1 = \begin{bmatrix} 0 \\ sgn(\alpha_1) \cdot (R_1 \cdot (1 - \cos(|\alpha_1|)) + d_2 \cdot \sin(|\alpha_1|)) \\ (R_1 \cdot \sin(|\alpha_1|) + d_2 \cdot \cos(|\alpha_1|)) \end{bmatrix} \quad (5)$$

$$(hint: \ R_1 = Sr_1/\alpha_1)$$

  R_1 is the radius of the Unit 1 bending curve, Sr_1 is the length of the Unit 1 backbone, and d_2 is the thickness of the disc whose centroid is $node_2$. Meanwhile, the rotational matrix $\mathbf{B}_1$ and the position matrix of $node_1$ $\mathbf{P}_1^{base}$ are shown in Equations 6 and 7.

$$\mathbf{B}_1 = \begin{bmatrix} 1 & 0 & 0 \\ 0 & 1 & 0 \\ 0 & 0 & 1 \end{bmatrix} \quad (6)$$

$$\mathbf{P}_1^{base} = \begin{bmatrix} 0 & 0 & 0 \end{bmatrix}^{\mathbf{T}} \quad (7)$$

  According to the Equations 5, 6, and 7, the position matrix of $node_2$ in the base coordinate system $\mathbf{P}_2^{base}$ can be calculated in Equation 8.

$$\begin{aligned} \mathbf{P}_2^{base} &= \mathbf{B}_1 \times \mathbf{P}_2^1 + \mathbf{P}_1^{base} \\ &= \begin{bmatrix} 1 & 0 & 0 \\ 0 & 1 & 0 \\ 0 & 0 & 1 \end{bmatrix} \times \begin{bmatrix} 0 \\ sgn(\alpha_1) \cdot (R_1 \cdot (1 - \cos(|\alpha_1|)) + d_2 \cdot \sin(|\alpha_1|)) \\ (R_1 \cdot \sin(|\alpha_1|) + d_2 \cdot \cos(|\alpha_1|)) \end{bmatrix} + \begin{bmatrix} 0 \\ 0 \\ 0 \end{bmatrix} \\ &= \begin{bmatrix} 0 \\ sgn(\alpha_1) \cdot (R_1 \cdot (1 - \cos(|\alpha|)) + d \cdot \sin(|\alpha|)) \\ (R_1 \cdot \sin(|\alpha|) + d \cdot \cos(|\alpha|)) \end{bmatrix} \end{aligned} \quad (8)$$

- Unit 2

  For Unit 2, the relationship between the relative position matrix of $node_2$

and $node_3$ $\mathbf{P}_3^2$ and α_2 is shown in Equation 9.

$$\mathbf{P}_3^2 = \begin{bmatrix} sgn(\alpha_2) \cdot (R_2 \cdot (1 - \cos(|\alpha_2|)) + d_3 \cdot \sin(|\alpha_2|)) \\ 0 \\ (R_2 \cdot \sin(|\alpha_2|) + d_3 \cdot \cos(|\alpha_2|)) \end{bmatrix} \quad (9)$$

$$(hint: \ R_2 = Sr_2/\alpha_2)$$

R_2 is the radius of the Unit 2 bending curve, Sr_2 is the length of the Unit 2 backbone, and d_3 is the thickness of the disc whose centroid is $node_3$. Meanwhile, the rotational matrix $\mathbf{B}_2$ and the position matrix of $node_2$ $\mathbf{P}_2^{base}$ are shown in Equations 10 and 8.

$$\mathbf{B}_2 = \begin{bmatrix} 1 & 0 & 0 \\ 0 & \cos(\alpha_1) & \sin(\alpha_1) \\ 0 & -\sin(\alpha_1) & \cos(\alpha_1) \end{bmatrix} \quad (10)$$

According to the Equations 8, 9, and 10, the position matrix of $node_3$ in the base coordinate system $\mathbf{P}_3^{base}$ can be calculated in Equation 11.

$$\begin{aligned} \mathbf{P}_3^{base} &= \mathbf{B}_1 \times \mathbf{B}_2 \times \mathbf{P}_3^2 + \mathbf{P}_2^{base} \\ &= \begin{bmatrix} 1 & 0 & 0 \\ 0 & 1 & 0 \\ 0 & 0 & 1 \end{bmatrix} \times \begin{bmatrix} 1 & 0 & 0 \\ 0 & \cos(\alpha_1) & \sin(\alpha_1) \\ 0 & -\sin(\alpha_1) & \cos(\alpha_1) \end{bmatrix} \\ &\times \begin{bmatrix} 0 \\ sgn(\alpha_2) \cdot (R_2 \cdot (1 - \cos(|\alpha_2|)) + d_3 \cdot \sin(|\alpha_2|)) \\ (R_2 \cdot \sin(|\alpha_2|) + d_3 \cdot \cos(|\alpha_2|)) \end{bmatrix} \\ &+ \begin{bmatrix} 0 \\ sgn(\alpha_1) \cdot (R_1 \cdot (1 - \cos(|\alpha_1|)) + d_2 \cdot \sin(|\alpha_1|)) \\ (R_1 \cdot \sin(|\alpha_1|) + d_2 \cdot \cos(|\alpha_1|)) \end{bmatrix} \end{aligned} \quad (11)$$

- Unit 3

For Unit 3, the relationship between the relative position matrix of $node_3$

and $node_4$ $\mathbf{P}_4^3$ and α_3 is shown in Equation 12.

$$\mathbf{P}_4^3 = \begin{bmatrix} 0 \\ sgn(\alpha_3) \cdot (R_3 \cdot (1 - \cos(|\alpha_3|)) + d_4 \cdot \sin(|\alpha_3|)) \\ (R_3 \cdot \sin(|\alpha_3|) + d_4 \cdot \cos(|\alpha_3|)) \end{bmatrix} \quad (12)$$

$$(hint: \ R_2 = Sr_2/\alpha_2)$$

R_3 is the radius of the Unit 3 bending curve, Sr_3 is the length of the Unit 3 backbone, and d_4 is the thickness of the disc whose centroid is $node_4$. Meanwhile, the rotational matrix $\mathbf{B}_3$ and the position matrix of $node_3$ $\mathbf{P}_3^{base}$ are shown in Equations 13 and 11.

$$\mathbf{B}_3 = \begin{bmatrix} \cos(\alpha_2) & 0 & \sin(\alpha_2) \\ 0 & 1 & 0 \\ -\sin(\alpha_2) & 0 & \cos(\alpha_2) \end{bmatrix} \quad (13)$$

According to the Equations 11, 12, and 13, the position matrix of $node_4$ in the base coordinate system $\mathbf{P}_4^{base}$ can be calculated in Equation 14.

$$\begin{aligned} \mathbf{P}_4^{base} &= \mathbf{B}_1 \times \mathbf{B}_2 \times \mathbf{B}_3 \times \mathbf{P}_4^3 + \mathbf{P}_3^{base} \\ &= \mathbf{B}_1 \times \mathbf{B}_2 \times \begin{bmatrix} \cos(\alpha_2) & 0 & \sin(\alpha_2) \\ 0 & 1 & 0 \\ -\sin(\alpha_2) & 0 & \cos(\alpha_2) \end{bmatrix} \\ &\times \begin{bmatrix} 0 \\ sgn(\alpha_3) \cdot (R_3 \cdot (1 - \cos(|\alpha_3|)) + d_4 \cdot \sin(|\alpha_3|)) \\ (R_3 \cdot \sin(|\alpha_3|) + d_4 \cdot \cos(|\alpha_3|)) \end{bmatrix} + \mathbf{P}_3^{base} \end{aligned} \quad (14)$$

- Unit 4

  In summary, the position matrix of $node_5$ in the base coordinate system P_5^{base}can be represented by Equation 15.

$$\mathbf{P}_5^{base} = \mathbf{B}_1 \times \mathbf{B}_2 \times \mathbf{B}_3 \times \mathbf{B}_4 \times \mathbf{P}_5^4 + \mathbf{P}_4^{base} \quad (15)$$

Applying the corresponding transformations to the Equation 4 reveals the

patterns shown in Equation 17.

$$\mathbf{P}_{i+1}^{base} - \mathbf{P}_{i}^{base} = \prod_{n=1}^{i} \mathbf{B}_n \times \mathbf{P}_{i+1}^{i} \tag{16}$$

$$\mathbf{P}_{i+1}^{base} = \sum_{m=1}^{i} \left[\prod_{n=1}^{m} \mathbf{B}_n \times \mathbf{P}_{m+1}^{m} \right] \quad (\mathbf{P}_{1}^{base} = 0) \tag{17}$$

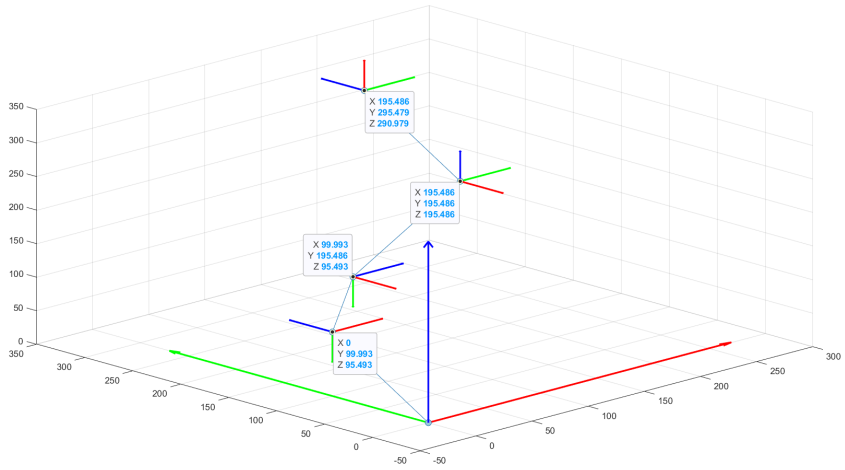

(a) $\alpha_1 = 90°, \alpha_2 = 90°, \alpha_3 = -90°, \alpha_4 = -90°$

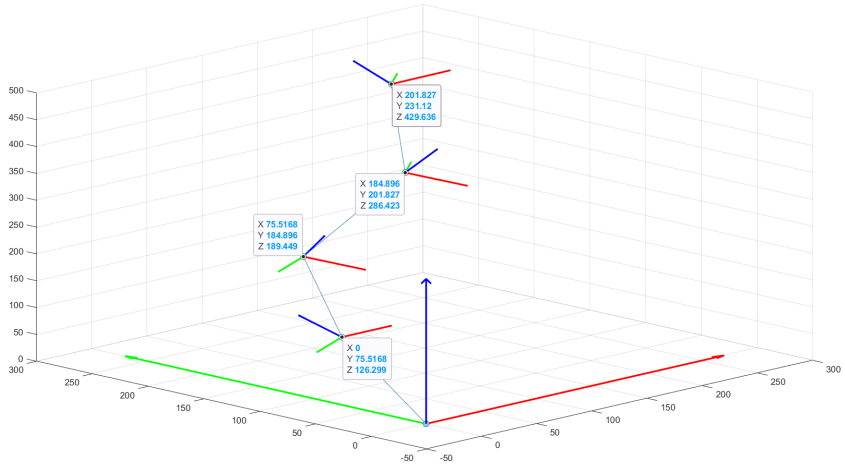

(b) $\alpha_1 = 60°, \alpha_2 = 60°, \alpha_3 = -60°, \alpha_4 = -60°$

Figure 7: ***The kinematics model of manipulator with respective bending units.***

4 Result and Discussion

This is the Result and Discussion of the final report.

4.1 part ??

unknown

4.2 part ??

unknown

4.3 part ??

unknown

4.4 part ??

unknown

4.5 part ??

unknown

4.6 part ??

unknown

4.7 part ??

unknown

4.8 part ??

unknown

4.9 part ??

unknown

4.10 part ??

unknown

4.11 part ??

unknown

5 Conclusion

This is the Conclusion of the final report.

References

[1] Ernar Amanov, Thien-Dang Nguyen, and Jessica Burgner-Kahrs. "Tendon-driven continuum robots with extensible sections—A model-based evaluation of path-following motions". In: *The International Journal of Robotics Research* 40.1 (2021), pp. 7–23.

[2] Ammar Amouri et al. "Bio-inspired a novel dual-cross-module sections cable-driven continuum robot: design, kinematics modeling and workspace analysis". In: *Journal of the Brazilian Society of Mechanical Sciences and Engineering* 45.5 (2023), p. 265.

[3] Tomer Anor, Joseph R. Madsen, and Pierre Dupont. "Algorithms for design of continuum robots using the concentric tubes approach: A neurosurgical example". In: *2011 IEEE International Conference on Robotics and Automation*. 2011, pp. 667–673. DOI: 10.1109/ICRA.2011.5980311.

[4] Jessica Burgner-Kahrs, D. Caleb Rucker, and Howie Choset. "Continuum Robots for Medical Applications: A Survey". In: *IEEE Transactions on Robotics* 31.6 (2015), pp. 1261–1280. DOI: 10.1109/TRO.2015.2489500.

[5] David Jakes, Zongyuan Ge, and Liao Wu. "Model-less Active Compliance for Continuum Robots using Recurrent Neural Networks". In: *2019 IEEE/RSJ International Conference on Intelligent Robots and Systems (IROS)*. 2019, pp. 2167–2173. DOI: 10.1109/IROS40897.2019.8968141.

[6] Sarthak Misra, K. T. Ramesh, and Allison M. Okamura. "Modeling of Tool-Tissue Interactions for Computer-Based Surgical Simulation: A Literature Review". In: *Presence* 17.5 (2008), pp. 463–491. DOI: 10.1162/pres.17.5.463.

[7] Priyanka Rao et al. “How to model tendon-driven continuum robots and benchmark modelling performance”. In: *Frontiers in Robotics and AI* 7 (2021), p. 630245.

[8] Matteo Russo et al. “Continuum robots: An overview”. In: *Advanced Intelligent Systems* 5.5 (2023), p. 2200367.

[9] Pan Zhou et al. “A bioinspired fishbone continuum robot with rigid-flexible-soft coupling structure”. In: *Bioinspiration & Biomimetics* 17.6 (2022), p. 066012.

Appendix A

TEST

This is the Appendix 1.

Appendix B

Test

This is the Appendix 2.